Available online at www.sciencedirect.com
ScienceDirect
Acta Materialia 58 (2010) 6421–6430
Acta MATERIALIA
www.elsevier.com/locate/actamat

Reinforcement architectures and thermal fatigue in diamond particle-reinforced aluminum

M. Schöbel [a,*], H.P. Degischer [a], S. Vaucher [b], M. Hofmann [c], P. Cloetens [d]

[a] Institute of Materials Science and Technology, Vienna University of Technology, Karlsplatz 13, A-1040 Vienna, Austria
[b] Advanced Materials Processing, EMPA – Swiss Federal Laboratories for Materials Science and Technology, Feuerwerkstrasse 39, CH-3602 Thun, Switzerland
[c] Forschungsneutronenquelle Heinz Maier-Leibnitz, Lichtenbergstrasse 1, D-85747 Garching, Germany
[d] European Synchrotron Radiation Facility, 6 Rue Jules Horowitz, F-38043 Grenoble, France

Received 26 May 2010; received in revised form 5 August 2010; accepted 5 August 2010
Available online 16 September 2010

Abstract

Aluminum reinforced by 60 vol.% diamond particles has been investigated as a potential heat sink material for high power electronics. Diamond (CD) is used as reinforcement contributing its high thermal conductivity (TC $\approx$ 1000 W mK^{-1}) and low coefficient thermal expansion (CTE $\approx$ 1 ppm K^{-1}). An Al matrix enables shaping and joining of the composite components. Interface bonding is improved by limited carbide formation induced by heat treatment and even more by SiC coating of diamond particles. An AlSi7 matrix forms an interpenetrating composite three-dimensional (3D) network of diamond particles linked by Si bridges percolated by a ductile α-Al matrix. Internal stresses are generated during temperature changes due to the CTE mismatch of the constituents. The stress evolution was determined in situ by neutron diffraction during thermal cycling between room temperature and 350 °C (soldering temperature). Tensile stresses build up in the Al/CD composites: during cooling <100 MPa in a pure Al matrix, but around 200 MPa in the Al in an AlSi7 matrix. Compressive stresses build up in Al during heating of the composite. The stress evolution causes changes in the void volume fraction and interface debonding by visco-plastic deformation of the Al matrix. Thermal fatigue damage has been revealed by high resolution synchrotron tomography. An interconnected diamond–Si 3D network formed with an AlSi7 matrix promises higher stability with respect to cycling temperature exposure.

Keywords: Particulate reinforced composites; Neutron diffraction; Synchrotron radiation computed tomography; Thermal cycling; Internal stresses

1. Introduction

Materials with high thermal conductivity (TC) in combination with a low coefficient of thermal expansion (CTE) are required for high power electronic devices in order to dissipate the heat from the chips to a heat sink [1]. Pure copper, a high conducting metal with a TC of ~400 W mK^{-1} but a relatively high CTE of ~17 ppm K^{-1}, which is commonly used, has been replaced by particle-reinforced composites such as AlSi7/SiC/70p (AlSiC) (for denotations see Table 1), which exhibit a reduced TC of ~250 W mK^{-1} and a CTE of ~8 ppm K^{-1} [2]. The CTE mismatch between the substrate and the ceramic base plate has to be small to avoid delamination of the solder at the interface due to thermal cycling during use. Increasing power densities demand increased efficiency in the thermal management of high power electronics. Diamond (CD) particles offer a good TC (~1000 W mK^{-1}) and a very low CTE (~1 ppm K^{-1}) [3,4] and could replace the SiC particles in AlSiC [5]. The large CTE mismatch between diamond and a metal matrix (Fig. 1) [6] produces high microstresses at the interfaces between the constituents during changes in temperature (Schöbel, Altendorfer, Degischer, Vaucher,

* Corresponding author. Tel.: +43 15880130836; fax: +43 15880130899.
E-mail address: michaels@mail.tuwien.ac.at (M. Schöbel).

1359-6454/$36.00 © 2010 Acta Materialia Inc. Published by Elsevier Ltd. All rights reserved.
doi:10.1016/j.actamat.2010.08.004

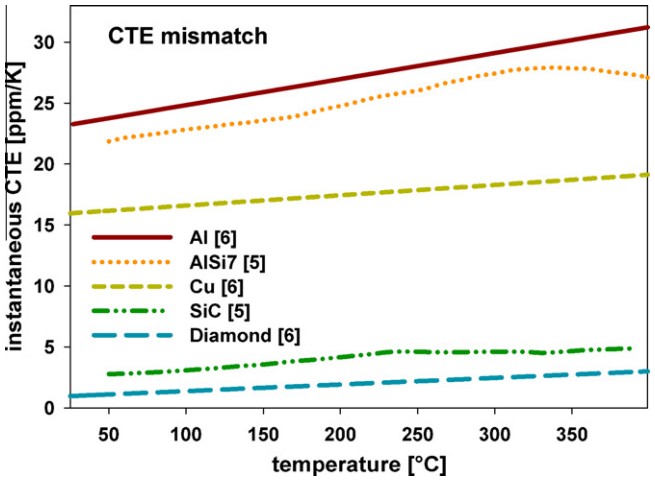

Fig. 1. CTE of Al and AlSi7 matrices, of the SiC and diamond reinforcements and of the composites AlSi7/SiC/70p and AlSi7/CD/60p compared with copper as a heat sink material.

Buslaps, Di Micheli and Hofmann, unpublished work). The use of a Cu matrix was unsuccessful, due to poor bonding with SiC and diamond particles [7]. The weak bonding of diamond with metal matrices needs to be improved to avoid interface delamination during thermal cycling [8]. Al may form interface carbides which improve bonding [4]. Interface reactions can be initiated by heat treatments just below the solidus temperature or by infiltrating SiC-coated diamond particles [9].

Pure Al and AlSi7 matrices have been investigated to determine whether AlSi7/CD/60p composites are stabilized by a three-dimensional (3D) reinforcement network such as in AlSi7/SiC/70p [5]. High particle volume fractions v_p are achieved by melt infiltration of densely packed particle preforms, which are compressed as much as possible by the non-wetting melt so that the particles touch each other [10,11]. The percolating solidified metal within the pores of the preform shrinks during cooling much more than the preform, due to the CTE mismatch between the metal matrix (CTE_m) and the ceramic particles (CTE_p). The volume difference in metal matrix composites (MMC) between the solid matrix v_m and the rigid particle arrangement can be estimated by Eq. (1) with reference to the volume fraction of the matrix [12]:

$$\Delta V(\Delta T) = 3v_m(\mathrm{CTE}_m - \mathrm{CTE}_p)\Delta T \quad (1)$$

Assuming a densely packed particle preform, the volume mismatch of the matrix with the interstices is determined by the volume fraction of the matrix v_m. The volume difference for Al in between 60 vol.% densely packed diamond particles reaches more than 2% during cooling from about 600 °C to room temperature (RT). A temperature change of 320 °C will result in a volume difference of about

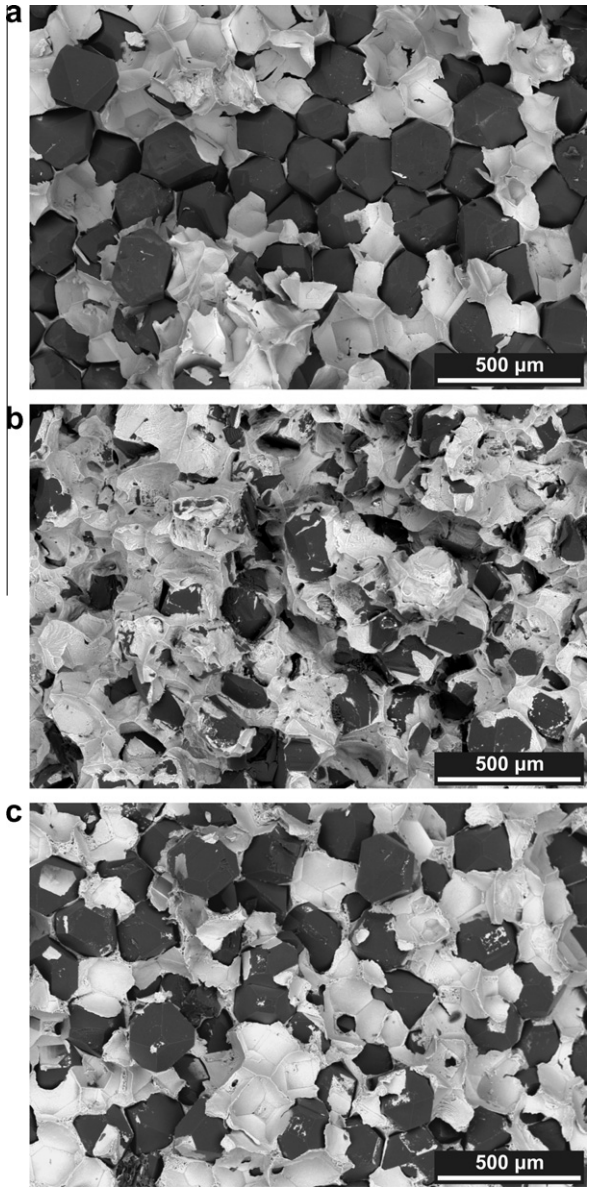

Fig. 2. BSE fractographs of (a) Al/CD/60p exhibiting mainly diamond particles (dark) free of matrix (bright), (b) AlSi7/CD/60p revealing mostly diamond particles covered by Al, and (c) Al/CD_{SiC}/60p showing fewer uncovered diamond particles than in (a).

Table 1
The diamond particle-reinforced Al composites investigated.

Composite	Matrix	Diamond particles (60 vol.%)	Condition
Al/CD/60p	Al 99.5%	Ø ≈ 200 or 25 µm	As cast
Al/CD/60p ht	Al 99.5%	Ø ≈ 200 or 25 µm	Heat treated, 640 °C, 5 h
Al/CD_{SiC}/60p	Al 99.5%	Ø ≈ 200 or 50 µm, SiC coated	As cast
AlSi7/CD/60p	Al + 7%Si	Ø ≈ 200 or 50 µm	As cast
AlSi7/CD_{SiC}/60p	Al + 7%Si	Ø ≈ 200 or 50 µm, SiC coated	As cast

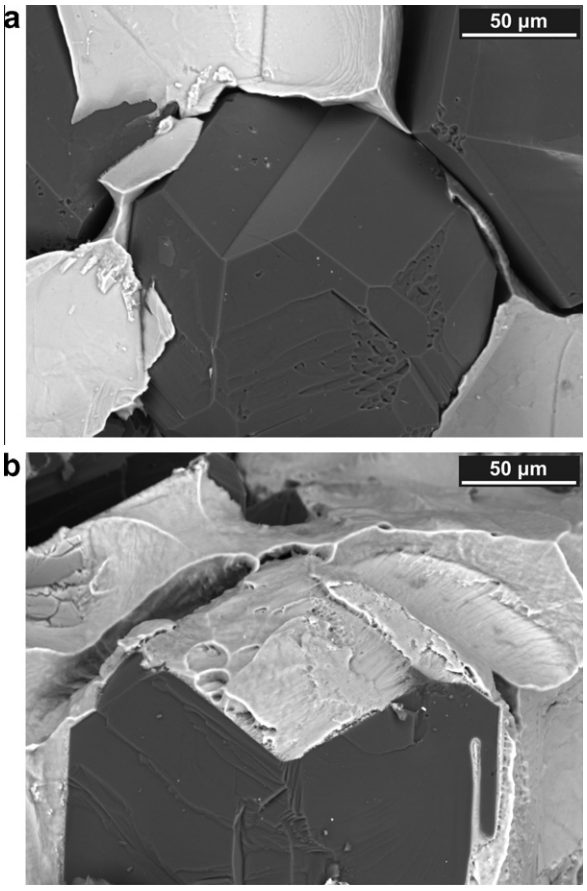

Fig. 3. BSE fractographs of pure Al/CD composites: (a) Al/CD/60p with faces of diamond (dark) and delaminated Al matrix (bright) and (b) Al adhering to SiC-coated diamond particles exhibiting micro-ductile deformation.

1 vol.%. Only a small fraction of deformation (<0.1%) can be accommodated by elastic strain. The resulting microstresses lead to delamination at the interfaces between the particles and the matrix and/or to pore formation within the matrix [12], even if perfectly infiltrated. If such damage was enhanced by thermal cycling it could cause advancing irreversible reduction of the thermal conductivity of the composite.

In a system with strong interface bonding, such as AlSiC, the initial void volume fraction changes during thermal cycling due to stress induced visco-plastic matrix deformation. The resulting void shrinkage produces an anomalous reduction in the CTE of AlSiC above ~200 °C (Schöbel et al., unpublished work). The Si in the AlSi7 matrix forms bridges between the SiC particles during solidification of the eutectic liquid connecting them to a permanent rigid Si–SiC structure [5]. The variation in the volume difference ΔV during heating and cooling is essentially accommodated by the changing void volume fraction. Superior long-term thermal fatigue resistance is expected for an interpenetrating composite compared with reinforcement by isolated particles [13]. Delamination and thermal fatigue damage is more probable in diamond-reinforced Al due to weaker interface bonding and a larger

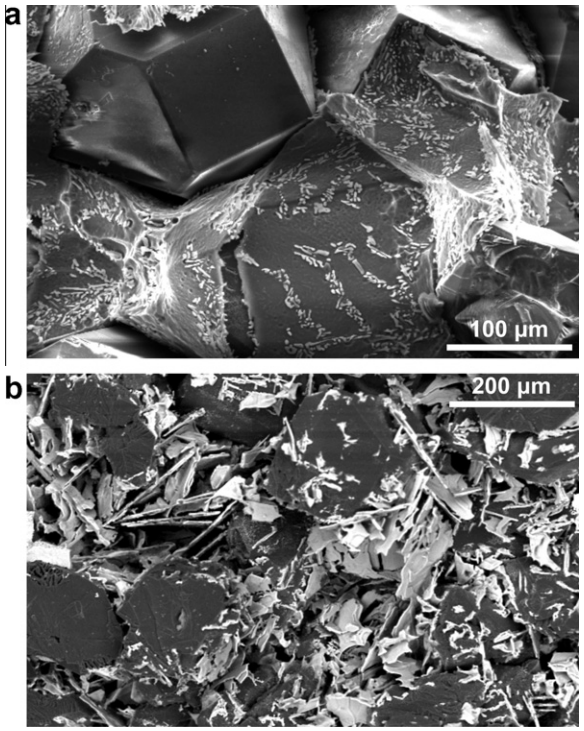

Fig. 4. BSE images of deep etched MMC showing Si bridges (bright) between the diamond particles (dark): (a) Si in AlSi7/CD/60p produced by squeeze casting at the Swiss Federal Laboratories for Materials Science and Technology [16] and (b) Si lamellae connecting the particles in AlSi11/CD/60p produced by gas pressure infiltration at Plansee Reutte, Austria (http://www.plansee.com).

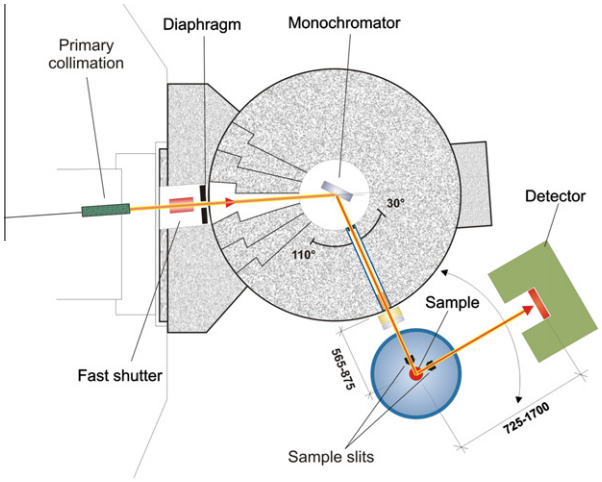

Fig. 5. Sketch of the Stress-Spec instrumental set-up at FRM2 [18]. A Ge single crystal monochromator produces thermal neutrons with a wavelength of $\lambda = 1.67$ Å using the Ge (5 1 1) lattice and a flux of 2×10^7 n cm^{-2} s^{-1} on the sample, $2\theta \approx 84.5$–88°, acquisition time 3 min.

CTE mismatch than in AlSiC composites. Improvements in interface bonding as well as the role of Si particles during thermal cycling are described here.

Neutron diffraction experiments [14] were performed to measure the microstresses between the matrix and diamond particles in situ during thermal cycling, similarly to previous studies on AlSiC (M. Schöbel et al., unpublished

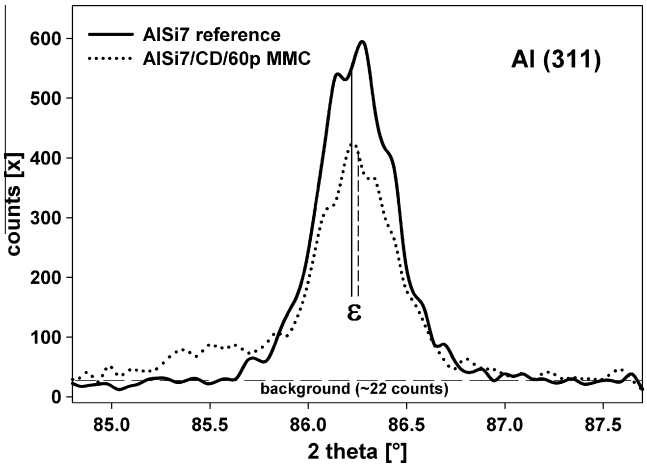

Fig. 6. Al (3 1 1) peak of the AlSi7/CD/60p composite compared with the Al matrix reference indicating the peak quality acquired within 3 min. Matrix strain (ε) in the composite was determined relative to the reference (unreinforced matrix).

work). Correlated in situ high resolution synchrotron tomography was used to visualize plastic deformation of the matrix due to changes in void volume fraction during thermal cycling.

2. Experimental procedure

2.1. Materials description

Diamond-reinforced Al composites were produced by melt infiltration of 60 vol.% monomodal particle preforms by squeeze casting at the Swiss Federal Laboratories for Materials Science and Technology [15]. Approximately 10 mm long cylindrical samples were prepared for neutron and synchrotron experiments with diameters of ~6 and ~0.8 mm, respectively as listed in Table 1. The same experimental set-up was used for the different composite samples to deliver comparable results. Reference measurements for strain determination were made on pure Al and AlSi7 matrix samples with the same dimensions to include the same superimposed macrostresses as in the composite samples and also to reduce diffraction surface effects.

Scanning electron microscopic back-scattered electron (BSE) images of fracture surfaces of Al/CD/60p, AlSi7/CD/60p and Al/CD_{SiC}/60p (with SiC-coated diamond particles) are shown in Fig. 2. The diamond particles (dark) were partly embedded in the Al matrix (bright). Micro-ductile dimples in the Al indicated good bonding to the SiC-coated diamond particles, as shown in Fig. 3. Si bridges connected the diamond particles in AlSi7/CD/60p, forming a 3D reinforcement network, shown in deep etched AlSi7/CD/60p and AlSi11/CD/60p in Fig. 4, in which the α-Al was leached out. The AlSi7 matrix finally solidified at thermodynamic equilibrium with a 50% AlSi12 eutectic liquid. The grain size of the matrix was in the range 50–500 μm (larger for a pure Al than a AlSi7 matrix). Small diamond particles (Ø ~ 25 and 50 μm) were used for the small tomography samples.

2.2. Neutron diffraction

Neutron diffraction was carried out in a Stress-Spec instrument in the high flux source FRM2, Garching, Germany [16]. A monochromatic neutron beam delivered by a Ge monochromator produces thermal neutrons with a wavelength of $\lambda = 1.67$ Å using the Ge (5 1 1) lattice and a flux of 2×10^7 n cm^{-2} s^{-1} on the sample. The Stress-Spec set-up (Fig. 5) allows strain scans on the Al (3 1 1) lattice planes in the matrix of the composites with an acquisition time of ~3 min in a ~125 mm^3 gauge volume almost completely covering the cross-section of the sample. Unidirectional scans were sufficient, due to the spherical symmetry of the strain system of the particle-reinforced composites (particle size ≪ gauge volume) (M. Schöbel et al., unpublished work). A representative volume is necessary to sample a statistically relevant number of grains contributing to the diffraction peak of the coarse grained matrix. The smaller gauge volumes of synchrotron diffraction would be dominated by crystal texture. The different composites were thermally cycled twice between RT and

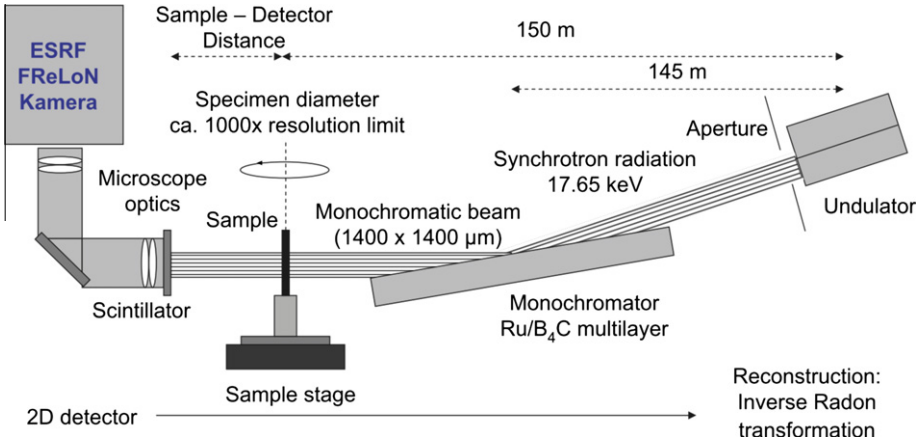

Fig. 7. The tomography set-up of the ID19 beam line at ESRF, Grenoble (http://www.esrf.fr). Parallel monochromatic beam set-up, with 900 images taken during a 180° rotation, CCD camera (2048 × 1024 pixels) in ROI scan mode with 0.3 μm^3 per voxel in binning mode.

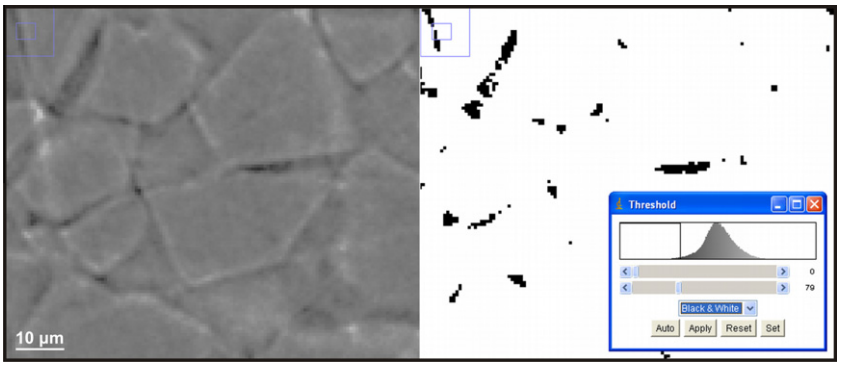

Fig. 8. An image slice from a tomographic scan of AlSi7/CD/60p: (left) reconstructed raw data with dark areas between the diamond particles representing voids and; (right) voids >27 voxels segmented below the threshold value in the histogram.

350 °C (soldering temperature) as in previous synchrotron experiments with the AlSiC composite in ID15A (M. Schöbel et al., unpublished work). The samples were heated by thermal contact with a heating wire and the temperature was measured with a thermocouple mounted on the specimen. Temperature cycles were controlled with a proportional integral derivative controller. The temperature was held constant for ~5 min, longer than the acquisition time (3 min) for isothermal diffraction measurements. The reference measurements on the matrix samples were made under the same conditions using the same set-up. During all experiments the 2D ^{3}He detector (256 × 256 pixels) was set to 82.5° (center position), including Al (3 1 1) at $2\theta \sim 86°$. Vertical summation over the counts gave the peaks relative to the reference (Fig. 6).

The elastic strains were determined in situ during thermal cycling for calculation of the matrix stress as a function of temperature. The gauge volume containing several dia-

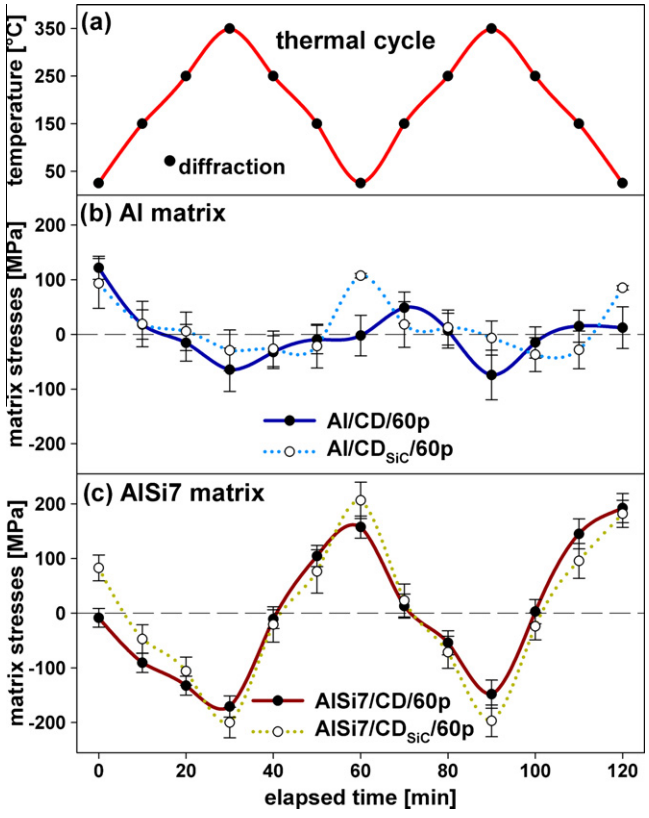

Fig. 9. (a) Microstresses during two thermal cycles of RT to 350 °C, (b) in pure Al matrix with weakly bonded Al/CD/60p and in Al/CD$_{SiC}$/60p with SiC-coated diamond particles, and (c) in α-Al of the AlSi7 matrix with uncoated particles (AlSi7/CD/60p) and SiC-coated particles (AlSi7/CD$_{SiC}$/60p).

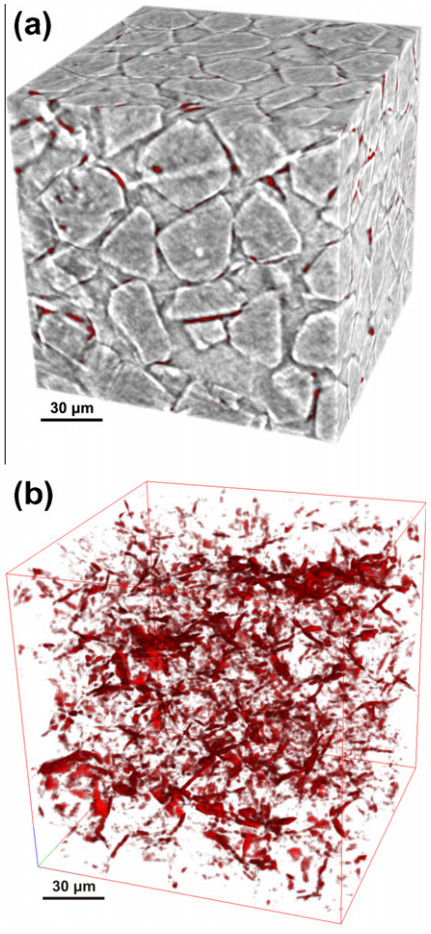

Fig. 10. Three-dimension view of a microtomographic image with (0.6 µm)^3 per voxel of an AlSi7/CD/60p cube of 140 µm^3 under the initial conditions at RT: (a) voids (dark) between the diamond particles mainly at the interfaces and (b) segmentation of voids >5 µm^3 amounting to a volume fraction of 1.6 vol.%.

mond particles embedded in the matrix gave an averaged matrix strain value. The three principal strain orientations ε_i exhibit spherical symmetry with particle sizes smaller than the gauge volume, as shown in a previous work (M. Schöbel et al., unpublished work). Simplification of Eq. (2a) allows calculation of the stress σ from one strain value ε (Fig. 6) according to Eq. (2b) using an isotropic Young's modulus $E(T)$ and Poisson ratio υ:

$$\sigma_i = \frac{E(T)\varepsilon_i}{(1+\upsilon)} + \frac{E(T)\upsilon(\varepsilon_1+\varepsilon_2+\varepsilon_3)}{(1+\upsilon)(1-2\upsilon)} \tag{2a}$$

$$\sigma = \frac{E(T)\varepsilon}{(1-2\upsilon)} \tag{2b}$$

These averaged values gave comparable matrix microstress results for the different composites for the same temperature variation, affected by the interface bonding quality and reinforcement architecture. Error values were produced by statistically fitting combined errors from the composite and reference measurements generated by the peak fit software [17].

2.3. Synchrotron tomography

High resolution synchrotron tomography experiments were performed in the ID19 tomography beam line at ESRF, Grenoble, France (http://www.esrf.fr), firstly to visualize the initial void volume fraction at the interfaces between the particles and the matrix and secondly to determine the changes in volume fraction in situ during thermal cycling. A small furnace set-up was used to place the sample as near as possible to the camera optics in order to reduce the phase contrast contribution. A coaxial thermocable heated the sample holder. The temperature was controlled by a thermocouple mounted on the sample at the lower end of the gauge volume. The tomograms were acquired in situ during thermal cycling over the same temperature steps and intervals as for the neutron diffraction experiment to deliver corresponding results.

The monochromatic beam travelled through the sample and was recorded by a high resolution charge-coupled device (CCD) camera behind the sample (Fig. 7). Nine hundred absorption contrast images (2048 × 1024 pixels) were acquired during rotation of the sample through 180° in the beam for each tomographic image. Region of interest scans (0.6 × 0.6 × 0.3 mm) in the center of the samples (Ø ~ 0.8 mm) delivered high resolution images. Absorption contrast was preferred for void segmentation. The phase contrast of the diamond surfaces was reduced to suppress superimposition on the void absorption contrast, but still show the outline of the particles. The binning mode was

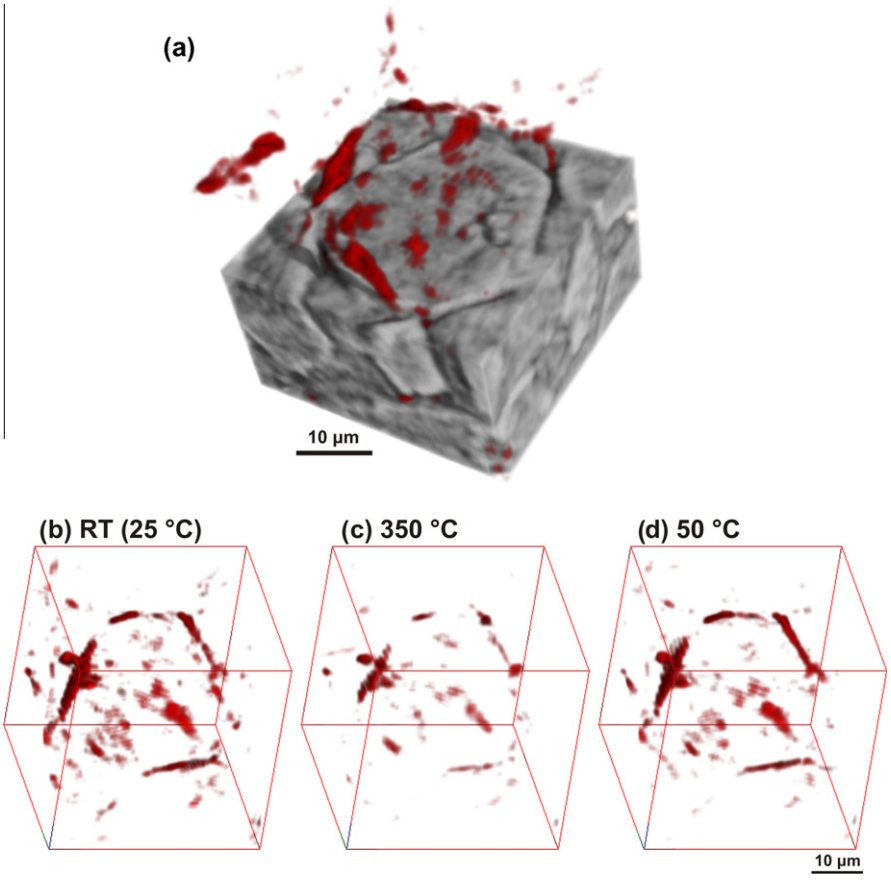

Fig. 11. Three-dimension view of microtomographic images with 0.6 µm^3 per voxel of an AlSi7/CD/60p cube of 40 µm^3: (a) diamond particles in the lower half of the cube and dark voids in the upper half under the initial conditions at RT, (b) segmented voids in the same region at RT, (c) the same voids segmented at 350 °C, and (d) at RT after cooling again during the first thermal cycle.

applied to the recording at 0.3 μm^3 per voxel, yielding a reconstructed voxel size of 0.6 μm^3 corresponding to the sum of four pixels, allowing a short acquisition time of ~3 min for each tomographic scan. A contrast resolution of $3 \times 3 \times 3$ voxels provides a void detectability of >5 μm^3 (M. Schöbel et al., unpublished work) or detectability of debonding gaps for delamination of >2 μm.

Image motion and ring artefacts were corrected before image reconstruction. The 32-bits 3D volumes were reduced to 8 bits by using only a defined gray value interval centered on the mean value of the 32-bits histogram. This avoids systematic segmentation errors due to brightness drifts between different scans. Void segmentation was carried out by setting a threshold value which was used for the image analysis of all scans in the same way (Fig. 8). Void volume segmentation was performed by voxel counting below the defined gray value, giving quantitative void volume fractions (M. Schöbel et al., unpublished work) only of those voids larger than the resolution limit (~5 μm^3). Image registration of the different scans using a registration software tool developed for similar problems [18] allowed region of interest visualization during thermal cycling. Registration was necessary due to sample drift on thermal expansion of the specimen and its mounting. A voxel to voxel correlation for scans recorded during thermal cycling was achieved. The error in void volume fraction of the resolved size class was calculated from the average deviation [18] of the voids segmented using the gray values adjacent to the selected threshold. The slope of the histogram at the chosen threshold gives the corresponding sensitivity of the void volume determination within the segmented volume.

3. Results

Neutron diffraction revealed the internal matrix microstresses in the different composites investigated in situ during thermal cycling between RT and 350 °C. Two cycles were performed to show stress evolution from the beginning, under the initial conditions of the composites at RT, compared with the stresses after the first cycle. Fig. 9 compares the matrix microstress evolution in Al between the composite systems Al/CD/60p, Al/CD$_{SiC}$/60p, AlSi7/CD/60p, and AlSi7/CD$_{SiC}$/60p. There remains some uncertainty about the absolute stress values, including the zero level in the range ±50 MPa (peak offset if sample > gauge volume), with a higher relative accuracy given by the error bars. Compressive stresses built up during heating, reaching a maximum at the peak temperature, when they became extremely high in the case of the AlSi7 matrix. Those stresses decreased during cooling and reverted to tension. The tensile stresses were higher in the Al matrix in which bonding of the diamond particles was enhanced by SiC coating during cooling compared with the uncoated system, but significantly lower than in the AlSi7 matrix composites.

A different matrix stress evolution was observed in the composites with a pure Al matrix (Fig. 9b) and a AlSi7 matrix (Fig. 9c). Initially the AlSi7 matrix stresses were similar to those of the pure Al matrix, but changed during heating to high hydrostatic compression, reaching ~200 MPa at 350 °C in both AlSi7/CD/60p and AlSi7/CD$_{SiC}$/60p. The stresses reverted during cooling to <250 °C, reaching ~200 MPa tension in the Al matrix at RT, explicable by hydrostatic conditioning. A slightly higher matrix stress amplitude was observed in AlSi7/CD$_{SiC}$/60p compared with AlSi7/CD/60p, originating from the higher interface bonding strength of the coated diamond particles.

An AlSi7/CD/60p cube of 140 μm^3 with a voxel size of 0.6 μm^3 is shown in Fig. 10. Dark voids appear in between the particles, mainly arranged at the interfaces. An initial void volume fraction of ~1.6 vol.% was identified in

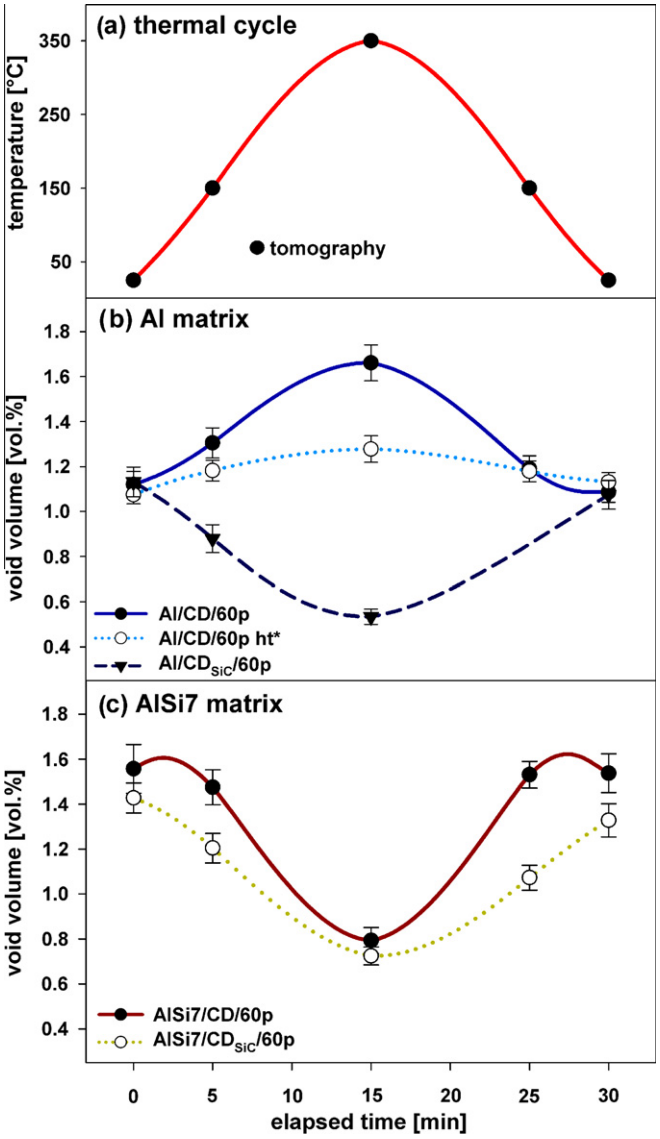

Fig. 12. (a) Quantitative tomographic results of segmented void volume fractions in a 200 μm^3 cube during one thermal cycle, (b) in pure Al matrix composites with different interface bonds (*interface reaction on heat treatment at 640 °C for 5 h), and (c) in AlSi7 matrix composites with SiC-coated and uncoated diamond particles.

AlSi7/CD/60p by the described segmentation at RT. Image registration identified the same region of interest from different scans visualized during thermal cycling. A volume of 40 μm^3 around a single diamond particle within the bulk material is shown in Fig. 11. The voids at the interfaces changed in volume during thermal cycling. In AlSi7/CD/60p the voids reversibly closed during heating and reopened during cooling. A larger volume of $\sim$200 μm^3 was chosen for a representative determination of the void volume fraction in Fig. 12. In the pure Al matrix of Al/CD/60p the voids opened during heating and closed during cooling. The voids remained at an almost constant volume fraction in the heat-treated composite (640 °C for 5 h). The change in void volume fraction in Al/CD_{SiC}/60p was the inverse of that for Al/CD/60p with an amplitude of 0.6 vol.%: voids shrank during heating and reopened during cooling. This was more pronounced in AlSi7/CD/60p and AlSi7/CD_{SiC}/60p, where the voids closed during heating and reopened during cooling with a change in volume fraction of 1 vol.% independent of the SiC coating.

4. Discussion

Voids exist in metal matrix composites produced by melt infiltration of densely packed particle preforms [10], even if perfectly infiltrated. The CTE mismatch between diamond and Al, increasing from 23 to 35 ppm K^{-1} between the ambient and melting temperature of the matrix, produced a volume difference of $\sim$2% for an Al matrix between 60 vol.% particles during cooling from $\sim$600 °C to RT. Microstresses built up in the composite, which could not accommodate the volume difference elastically. Creep

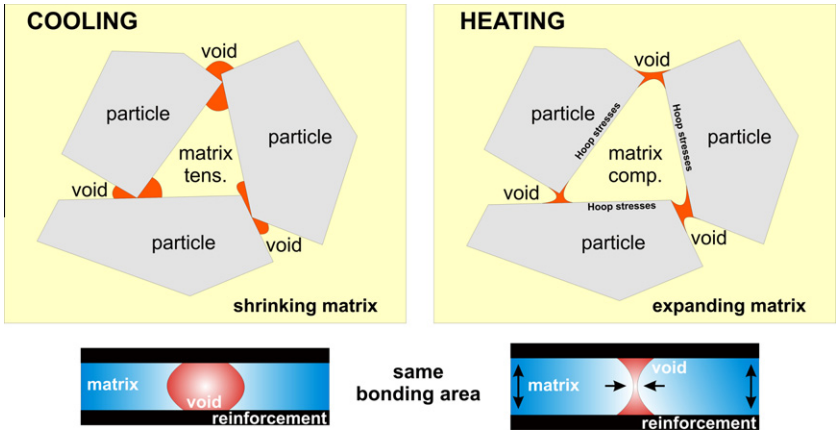

Fig. 13. Isolated particles bonded in a matrix with shrinkage pores in between the particles formed during cooling after infiltration (left). Matrix expansion during heating (right) produced Hoop compression, pressing the soft matrix into the voids. During cooling matrix tension (left) in between the well-bonded touching particles reopened these voids. Changes in void volumes with stable interface contact.

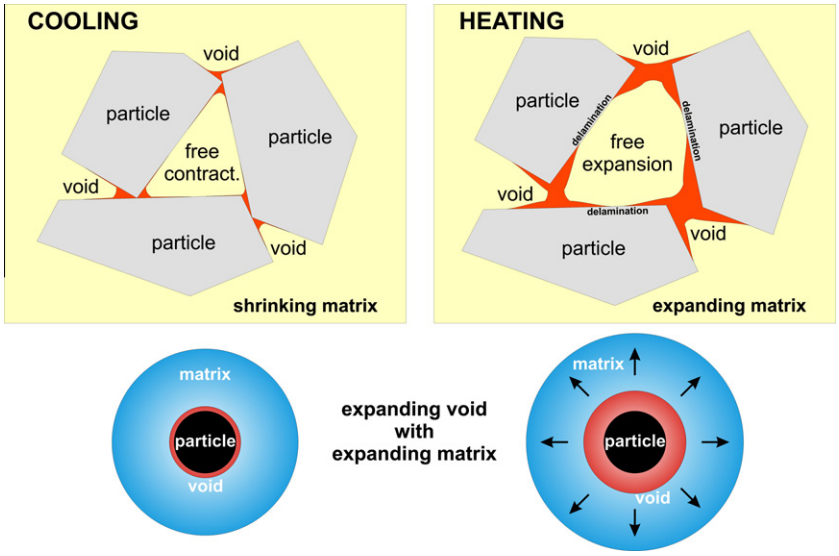

Fig. 14. Isolated particles weakly bonded in a matrix with infiltration voids and regional delaminated interfaces (left). Free matrix expansion was hindered by touching particles but not by weak bonding of particles during heating (right). Voids were opened by expansion of the matrix sponge. During cooling the shrinking Al matrix was pressed onto the particles, closing the voids.

deformation of Al will take place at elevated temperatures and the matrix yield strength may be surpassed approaching RT. Tensile stresses were expected after processing, which may relax during storage. The initial tensile stress level in Al was similar for all the composites investigated. It increased after cooling from 350 °C in the AlSi7 composites.

Figs. 13–15 illustrate the thermal cycling stress situation and the changes in void volume schematically for densely packed diamond particles with and without interface bonding and Si bridges between the particles.

Fig. 13 indicates a stable interface with the pore surfaces changing from concave after cooling to convex during heating [19]. Circumferential Hoop tension built up in the Al close to the interface with the coated diamond particles approaching RT (Al/CD_{SiC}/60p in Fig. 9b). The void volume fraction decreased during heating due to the inversion from tensile stress to compression (Al/CD_{SiC}/60p in Fig. 12b). Although some delamination at the interfaces was observed, there was strong bonding between the SiC-coated diamond particles and the matrix.

In contrast, the pure Al between uncoated diamond particles exhibited low stress amplitudes (Al/CD/60p in Fig. 9b). A porous sponge-like Al matrix, as shown in Fig. 14 is assumed, with the diamond particles within the pores. The Al sponge expanded during heating, hindered by the stable diamond particles, so that compressive stresses built up. Microtomography revealed an increase in void volume fraction during heating as a consequence of the freely expanding sponge (Al/CD/60p in Fig. 12b). The opposite occurred during cooling, creating tensile stresses, which closed the voids.

The composites containing Si in the matrix alloy, AlSi7/CD/60p and AlSi7/CD_{SiC}/60p, formed an interpenetrating structure, with the diamond particles in the matrix connected by Si bridges during solidification of the Al–Si eutectic liquid (Fig. 4). The Si–diamond network formed a rigid open porous cage permeated by α-Al (Fig. 15). The matrix Al shrank during cooling, opening voids to accommodate the volume difference (Fig. 10b). The corresponding hydrostatic tensile stresses relaxed by creep during storage. Only interface bonding with the SiC-coated diamond particles maintained some tensile Hoop stresses. Hydrostatic compression stresses built up during heating due to matrix expansion constrained by the reinforcement network (Fig. 9c). These relatively high multi-axial stresses led to visco-plastic matrix deformation at high temperatures, closing the voids (Figs. 11 and 12c). During cooling from 350 °C stress inversion could be observed at <250 °C, leading to Al matrix tension at RT reopening the voids. The microstress evolution in AlSi7/CD/60p was similar to that in AlSi7/CD_{SiC}/60p, with a slightly higher stress amplitude due to the stronger bonding provided by the SiC coating on the diamond particles. Improved bonding by SiC-coated diamonds in the AlSi7 matrix only increased the residual stresses and may not be necessary for stability of such an interpenetrating composite.

However, improved bonding due to SiC coating of the diamond particles in the permeating pure Al matrix produced similar changes in void volume fraction as in the AlSi7/CD/60p samples. Debonding of the particles from the metal matrix would reduce the thermal conductivity of the composite. In the interconnected Si–CD structure of AlSi7/CD/60p the dominant compression prevented debonding during heating. The long-term stability may be increased by an interconnected network of reinforcements with interface regeneration at high temperatures, compared with a system of isolated particles. Furthermore,

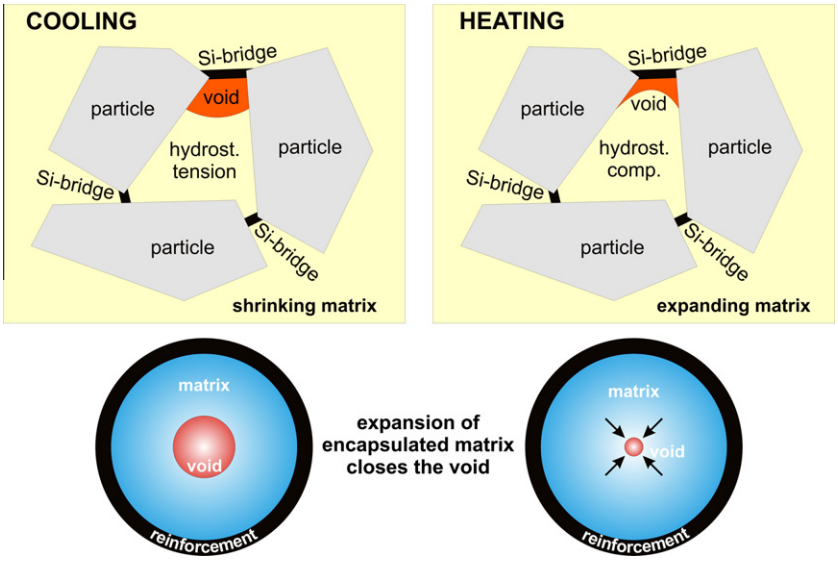

Fig. 15. Matrix embedded in a cage of interconnected reinforcement network. Hydrostatic tension opened shrinkage pores during cooling after infiltration (left). During heating compression of the α-Al within the rigid reinforcement network closed the voids by visco-plastic matrix deformation (right). Matrix tension reopened the voids during cooling (left).

the reduction in void volume fraction during heating would partially accommodate the expanding ductile matrix, leading to a reduction in the macroscopic CTE, as observed for AlSiC (M. Schöbel et al., unpublished work).

5. Conclusions

- Voids form in diamond-reinforced aluminum during cooling from melt infiltration of densely packed diamond particle preforms. Shrinkage of the aluminum matrix between the thermally stable touching diamond particles produces a volume difference of about 2%, which has to be accommodated by delamination and void formation.
- If bonding between particles and matrix is poor, as it usually is between pure Al and uncoated diamond particles, reheating the permeating matrix increases the void volume fraction by free expansion of a ductile matrix foam.
- The bonding can be improved by heat treatment below the solidus temperature, causing the formation of interface Al carbides. Significantly stronger bonding is achieved by infiltration of SiC-coated diamond particles. Tensile Hoop stresses are built up approaching room temperature. The SiC coating causes advantageous void shrinkage during heating.
- Si particles originating from solidification of the interdendritic eutectic liquid, which accounts for 50% of the matrix, connect the diamonds, producing an interpenetrating composite with a 3D network of diamond particles connected by Si between the permeating α-Al. The internal stresses in the Al matrix become compressive during heating and tensile during cooling, creating favorable void closing at elevated temperatures (M. Schöbel et al., unpublished work). If there were no voids, the composite would be likely to break up during heating owing to the volume mismatch.

Thermal fatigue damage occurs particularly during the soldering process, where the electronic packaging is heated to about 350 °C and rapidly cooled. The thermal cycles during service range between −50 °C and +150 °C and might be harmful with increasing number of cycles. An interconnected Si–CD structure in an AlSi7 matrix produces isotropic matrix compression during heating, by which voids and delaminations are closed, so improving conductivity. Tensile stresses induce debonding during cooling by matrix shrinkage, where lower conductivity is required. Thermal fatigue damage propagation may be reduced in AlSi7 matrix systems by creation of an interpenetrating composite, in contrast to the pure Al matrix system with densely packed isolated particles, in which the voids grow with increasing temperature.

Acknowledgements

The research was financed by the ExtreMat 6th framework EU project, and the authors would like to thank all the cooperating partners. Special thanks are due to Manjusha Battabyal for cooperation in the sample preparation. Last but not least, we thank the staffs of FRM2 Garching, Germany, and ESRF Grenoble, France, for their support in helping with, organizing and carrying out the experiments on their sites.

References

[1] Zweben C. J Metal 1992;44:15–23.
[2] Lefranc G, Degischer HP, Sommer HK, Mitic G. In: Massard T, editor. ICCM12 proceedings, ICCM association, Paris; 1999.
[3] Battabyal M, Beffort O, Kleiner S, Vaucher S, Rohr L. Diam Relat Mater 2008;17:1438–42.
[4] Kleiner S, Khalid FA, Ruch PW, Meier S, Beffort O. Sci Mater 2006;55(4):291.
[5] Huber T, Degischer HP, Lefranc G, Schmitt T. Comp Sci Technol 2006;66:2206–17.
[6] Joseph A, King I. Materials handbook for hybrid microelectronics. Norwood, USA; 1988.
[7] Schubert T, Ciupinski L, Zielinski W, Michalski A, Weißgärber T, Kieback B. Sci Mater 2008;58:263–6.
[8] Beffort O, Khalid FH, Weber L, Ruch P, Klotz UE, Meier S, et al. Relat Mater 2006;15(9):1250.
[9] Leparoux S, Diot C, Dubach A, Vaucher S. Sci Mater 2007;57:595–7.
[10] Mortensen A. In: Kelly A, Zweben C, editors. Metal matrix composites, vol. 3. Oxford (UK): Pergamon Press; 2000. p. 541–7.
[11] Clyne TW. Encyclopedia of materials science and technology. Oxford: Elsevier; 2001.
[12] Degischer HP, Lasagni F, Schöbel M, Huber T, Aly MA. In: International conference on advanced materials, ICAMC proceedings, NIIST, Trivandrum-695019, India; 2007.
[13] Schöbel M, Fiedler G, Degischer HP, Altendorfer W, Vaucher S. Adv Mater Res 2009;59:177–81.
[14] Hofmann M, Skirl S, Pompe W, Rödel J. Acta Mater 1999;47(2):565–77.
[15] Beffort O, Vaucher S, Khalid FA. Diam Relat Mater 2004;13:1834–43.
[16] Hofmann M, Schneider R, Seidl GA, Rebelo-Kornmeier J, Wimpory RC, Garbe U, et al. Physica B 2006:385–6. 1035–7.
[17] Fitzpatrick ME, Lodini A. Analysis of residual stress by diffraction using neutron and synchrotron radiation. London: Taylor & Francis; 2003.
[18] Altendorfer W. Diploma thesis, Institute for Computer Graphics and Algorithms. Austria: Vienna University of Technology; 2008.
[19] Nam TH, Requena G, Degischer HP. Composites Part A 2008;39:856–65.